Mon. Not. R. Astron. Soc. **000**, 000–000 (0000) Printed 12 February 2022 (MN LATEX style file v2.2)

Unveiling the birth and evolution of the H II region Sh2-173

S. Cichowolski,[1⋆] G.A. Romero,[2,3] M.E. Ortega,[1]† C.E. Cappa, [2⋆] and J. Vasquez,[2] ‡

[1] *Instituto de Astronomía y Física del Espacio (IAFE), CC 67, Suc. 28, 1428 Buenos Aires, Argentina*

[2] *Instituto Argentino de Radioastronomía (CCT-La Plata, CONICET), CC 5, 1894 Villa Elisa, Argentina and Facultad de Ciencias Astronómicas y Geofísicas, Universidad Nacional de La Plata, Paseo del Bosque s/n, 1900 La Plata, Argentina*

[3] *Departamento de Física y Astronomía, Facultad de Ciencias, Universidad de Valparaiso, Valparaiso, Chile*

arXiv:0812.3872v1 [astro-ph] 19 Dec 2008

ABSTRACT

Based on a multiwavelength study, the interstellar medium around the H II region Sh2-173 has been analyzed. The ionized region is clearly detected in the optical and in the radio continuum images. The analysis of the H I data shows a region of low emissivity that has an excellent morphological correlation with the radio continuum emission. The H II region is partially bordered by a photodissociation region, which, in turn, is encircled by a molecular structure. The H I and CO structures related to Sh2-173 are observed in the velocity ranges from –25 to –31$\mathrm{km\,s^{-1}}$, and from –27 to –39 $\mathrm{km\,s^{-1}}$, respectively. Taking into account the presence of noncircular motions in the Perseus spiral arm, together with previous distance estimates for the region, we adopt a distance of 2.5 $\pm$ 0.5 kpc for Sh2-173. Seven hot stars were identified in the field of Sh2-173, being only one an O-type star. The amount of energetic photons emitted by this star is enough to keep the region ionized and heat the dust. Given that an expanding H II region may trigger star formation, a search for YSO candidates was made using different infrared point source catalogues. A population of 46 YSO candidates was identified projected onto the molecular clouds.

On the other hand, Sh2-173 is located in a dense edge of a large ($\sim 5^\circ$) H I shell, GSH 117.8+1.5-35. The possibility for Sh2-173 of being part of a hierarchical system of three generations is suggested. In this scenario, the large H I shell, which was probably originated due to the action of Cas OB5, would have triggered the formation of Sh2-173, which, in turn, is triggering new stars in its surrounding molecular cloud. To test this hypothesis, the ages of both, the H II region and the large shell, were estimated and compared. We concluded that Sh2-173 is a young H II region of about 0.6 - 1.0 Myr old. As for the large shell we obtained a dynamical age of 5 $\pm$ 1 Myr. These age estimates, together with the relative location of the different structures, support the hypothesis that Sh2-173 is part of a hierarchical system.

Key words: ISM: individual:Sh2-173 – ISM: kinematics and dynamics – H II regions – stars: formation.

1 INTRODUCTION

Massive stars affect their environment by ionizing radiation, stellar winds, and, finally, supernova explosions. These stars produce intense extreme ultraviolet ($h\nu > 13.6$ eV) radiation, creating H II regions around them, and intense far ultraviolet ($4.5 < h\nu < 13.6$ eV) radiation that can penetrate into regions of molecular gas, dissociating it. They also have powerful winds which sweep up the surrounding gas creating what is known as an interstellar bubble, i.e. a minimum in the gas distribution characterized by a low volume density and a high temperature, surrounded by an expanding envelope (Weaver et al. 1977). In the case of OB associations, their collective effect has a huge impact in the surrounding interstellar medium (ISM), creating large structures of about hundred parsecs. Winds and supernova explosions transfer to the ISM vast amounts of mechanical energy, generating the compression of nearby molecular clouds. The effects of the massive stars are mostly destructive in their immediate neighborhood, since they tend to disrupt the parental molecular cloud. However, a little further away, massive stars stimulate star formation. A number of papers have been devoted to investigate star formation in the dense molecular clouds in the surroundings of H II regions, both from a theoretical and an observational point of view.

Different processes can trigger stellar formation at the pe-

⋆ Member of the Carrera del Investigador Científico of CONICET, Argentina
† Doctoral Fellow of CONICET, Argentina
‡ Post-Doc Fellow of CONICET, Argentina

riphery of H II regions (Elmegreen & Lada 1977; Klein et al. 1980; Sandford et al. 1982; Lefloch & Lazareff 1994; Whitworth et al. 1994; Lefloch & Lazareff 1995; Deharveng et al. 2005; Dale et al. 2007). Star formation can be induced in the environs of massive stars due to the action of expanding shocks which modify the surrounding material, either favouring the formation of cometary globules in preexistent clumps ("Radiative Driven Implosion" model, RDI) or sweeping up the surrounding material into a collected layer, which latter becomes gravitationally unstable generating massive fragments ("collect and collapse" model). Both processes, which may act simultaneously in an H II region, lead to the formation of a new generation of stars. Observational evidence of both (the RDI and "collect and collapse") processes has been found in a number of H II regions (e.g. Thompson et al. 2004; Deharveng & Zavagno 2008; Cappa et al. 2008; Kirsanova et al. 2008).

The goal of this paper is to achieve a better understanding of the phenomena associated with the interaction between young massive stars and their surrounding interstellar medium and, specifically, to attempt to shed some light on the process of triggered star formation. To carry out this study a multiwavelength approach is essential in order to obtain a complete picture of the different components of the ISM, the young stellar population, and the interactions among them.

In this work we investigate the environs of the H II region Sh2-173 by analyzing the distribution of the ionized and neutral material, and that of the interstellar dust. Sh2-173 is an optically visible H II region (Sharpless 1959) located at (*l*, *b*) = (119.°4, –0.°94) in the Perseus spiral arm. The DSS2-R image of Sh2-173 is displayed in Fig. 1. The region is approximately circular in shape with a diameter of about 30′. An arc-like structure of enhanced optical emission is evident on the north-west side of the region, while fainter emission is present at higher galactic longitudes and lower galactic latitudes. Inside the ionized region, two voids lacking optical emission are evident at (*l*, *b*) = (119.°4, –0.°85) and (*l*, *b*) = (119.°55, –0.°95). Russeil, Adami, & Georgelin (2007) identified seven hot stars in the field of Sh2-173, which are listed in Table1, and indicated with small triangles in Fig. 1. All of the stars but one are projected close to the center of the region. ALS 6155, on the contrary, is seen projected on its southeast border.

The distance to Sh2-173 has been estimated by several authors using independent methods. A spectrophotometric distance of 2.7 ± 0.9 kpc was derived by Georgelin (1975), while Russeil et al. (2007) estimated a distance of 3.12 ± 0.34 kpc based on UBV photometric and spectroscopic data of the exciting stars (see Table 1). Using a new method for determination of distances, which is based on H I column densities and is independent of Galactic kinematics, Foster & Routledge (2003) estimated for this H II region a distance of 2.2 ± 0.4 kpc. Blitz, Fich, & Stark (1982) in their CO survey towards H II regions found molecular gas related to Sh2-173 at –34.5 $\mathrm{km\,s^{-1}}$ (all the velocities are referred to the LSR). This velocity coincides with the radial velocity of the ionized gas derived from Fabry-Perot Hα observations, -34.3 ± 0.3 $\mathrm{km\,s^{-1}}$ (Fich, Dahl, & Treffers 1990). It is well known that noncircular motions on a large scale are present in the Perseus spiral arm (Brand & Blitz 1993). An inspection of Fig. 2b of Brand & Blitz (1993), which takes into account noncircular motions, suggests for a velocity of about –34 $\mathrm{km\,s^{-1}}$, a kinematical distance of 1.8-2 kpc. Thus, the distance of Sh2-173 is between 1.8 and 3.1 kpc. As a working hypothesis, we will adopt a distance of 2.5 ± 0.5 kpc for Sh2-173.

Sh2-173 is seen located in the dense border of a large H I shell

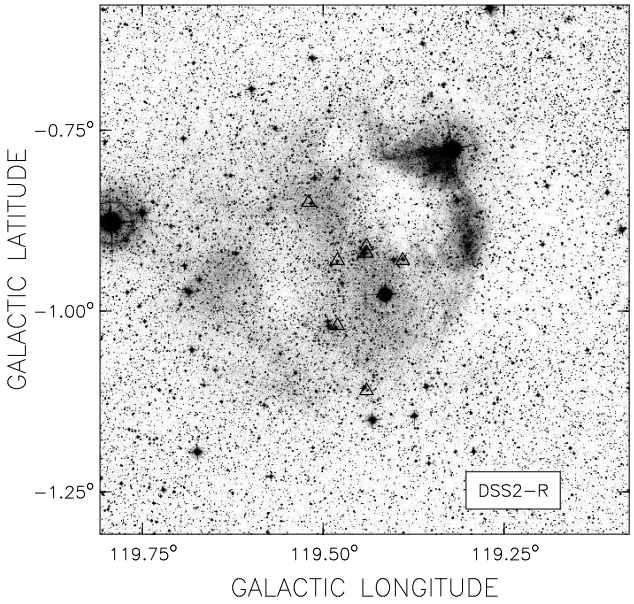


Figure 1. DSS2-R optical image of the H II region Sh2-173. The small triangles indicate the position of the seven OB stars listed in Table 1.

Table 1. Stellar parameters of the OB stars associated with Sh2-173.

Star	Spectral Type[1]	Galactic coordinates	Distance[1] [kpc]	Comments
ALS6145	B0.5V	119.°39, –0.°93	3.17 ± 1.27	
ALS6150	B2IV	119.°44, –0.°91	3.78 ± 1.89	
ALS6151	O9V	119.°44, –0.°92	2.57 ± 0.5	BD+60 39
ALS6155	B0.5V	119.°44, –1.°11	3.36 ± 1.34	
ALS6156	B2V	119.°48, –0.°93	4.41 ± 1.77	
ALS6157	B2IV	119.°48, –1.°02	2.27 ± 1.14	BD+60 42
ALS6158	B1V	119.°52, –0.°85	4.02 ± 0.66	

1- From Russeil et al. (2007).

($\sim 5^\circ$ diameter) that has been found in the Perseus spiral arm by Fich (1986) using Weaver & Williams (1973) H I data. Fich (1986) suggested that the presence of SNR remnants and several H II regions in the field indicates a great deal of star-formation activity going on nearby. Kiss, Moór, & Tóth (2004) found a far infrared ring close to the H I shell defined by Fich (1986). Heyer et al. (1998) found a large void of CO emission centered at (*l*, *b*) = (117.°6, 0.°0), coincident with the H I shell. Based on a multiwavelength study, Moór & Kiss (2003) determined the main parameters of the shell and associated it with the OB association Cas OB5 (≡ Rupr 33). According to Garmany & Stencel (1992), Cas OB5 has a zero-age main sequence (ZAMS) fairly good defined with a distance modulus DM = 11.5 mag (D $\sim$ 2 kpc). The diameter of the association is about 4°, or 140 pc at 2 kpc. Its earliest star is HD 108 (O6f). Among their members there are six O-type stars, being the others B stars (Garmany & Stencel 1992). A WN4 star (WR 159) was found in the area of Cas OB5, located at (*l*, *b*) = (115.°78, +1.°24) (Negueruela 2003).

Table 2. Observational parameters.

H I data:	
Synthesized beam ($\Theta_l \times \Theta_b$)	$1\farcm1 \times 1\farcm0$
Position angle[a]	97°
Velocity coverage	-164 to 44.7 $\mathrm{km\,s^{-1}}$
Channel separation	0.82 $\mathrm{km\,s^{-1}}$
Velocity resolution	1.3 $\mathrm{km\,s^{-1}}$
Observed rms noise (single channel)	1.3 K
Radio continuum at 408 MHz:	
Synthesized beam ($\Theta_l \times \Theta_b$)	$3\farcm2 \times 2\farcm8$
Position angle[a]	95°
Observed rms noise	0.5 K
Radio continuum at 1420 MHz:	
Synthesized beam ($\Theta_l \times \Theta_b$)	$0\farcm93 \times 0\farcm8$
Position angle[a]	97°
Observed rms noise	0.05 K
CO data:	
Angular resolution	$1\farcm67$
Velocity coverage	-150.7 to 38.9 $\mathrm{km\,s^{-1}}$
Velocity resolution	0.98 $\mathrm{km\,s^{-1}}$
Channel separation	0.82 $\mathrm{km\,s^{-1}}$
Observed rms noise (single channel)	0.2 K
Infrared data:	
HIRES	
Angular resolution	$0\farcm5$ - $2'$
MSX	
Angular resolution	$18\farcs4$

a Position angle measured CCW from the longitude axis.

2 DATA SETS

Radio continuum data at 408 and 1420 MHz, as well as 21-cm spectral line data, were obtained using the Dominion Radio Astrophysical Observatory (DRAO) interferometer as part of the Canadian Galactic Plane Survey (CGPS) (Taylor et al. 2003). The CGPS data base also comprises other data sets that have been reprojected and regridded to match the DRAO images. Among them are the IRAS high resolution (HIRES) data (Fowler & Aumann 1994) and the Five College Radio Astronomical Observatory (FCRAO) CO Survey of the Outer Galaxy (Heyer et al. 1998).

Radio continuum surveys at 325 MHz (WENSS) (Rengelink et al. 1997), 2695 MHz (Fürst et al. 1990), and 4850 MHz (Condon et al. 1994) were also used in this work.

Mid-infrared data were taken from the *MSX* Galactic Plane Survey (Price et al. 2001) and near-infrared data were obtained from the 2MASS All-Sky Point Source Catalog (Skrutskie et al. 2006).

Table 2 summarizes the most relevant observational parameters.

3 SH2-173 AND ITS LOCAL ISM

3.1 Ionized Gas

Figure 2 shows the radio continuum emission distribution at different wavelengths. The upper panel shows the radio emission at 408 MHz, while the image at 1420 MHz is shown in the middle panel. Clearly, the radio emission at 408 MHz is dominated by strong point like sources. An arc of strong radio continuum emission overlaying a more extended diffuse emission is observed at 1420 MHz.

Table 3. Radio continuum flux densities of Sh2-173.

Frequency (MHz)	Integrated flux density (Jy)
325	1.8 ± 1.0
408	1.3 ± 0.6
1420	1.8 ± 0.3
2695	1.8 ± 0.3
4850	1.6 ± 0.3

The radio emission extends towards higher galactic longitudes and lower galactic latitudes, slowly decreasing in brightness. The bottom panel displays an overlay of the emission at 1420 MHz (*line contours*) and the optical image (*grey-scale*). The arc-like structure is coincident with the brightest optical region. On the contrary, the relatively strong radio emission near (*l*, *b*) = (119.°4, –0.°85) is projected onto one of the regions lacking optical emission. The H II region shows a similar morphology at 325, 2695, and 4850 MHz.

To elucidate the nature of the numerous point sources observed in the field, we have used the available catalogued flux densities (The Texas Survey [365 MHz, (Douglas et al. 1996)], WENSS [325 MHz, (Rengelink et al. 1997)], NVSS [1420 MHz, (Condon et al. 1998)]). The derived spectral indexes ($S_\nu \sim \nu^\alpha$) are representative of extragalactic nonthermal radio sources. In particular, the strong radio source located at (*l*, *b*) = (119.°38, -0.°84), which is close to the bright part of Sh2-173, has a flux density of 235 mJy at 365 MHz and of 67.1 mJy at 1420 MHz, resulting in a spectral index $\alpha \sim -0.9$. The contribution of the compact sources projected onto the H II region was subtracted in order to properly estimate the flux density of the ionized region. The derived flux densities of Sh2-173 are listed in Table 3. The least square fitting of these values gives a spectral index $\alpha = 0.0 \pm 0.1$, confirming that the extended source is an H II region.

The parameters of the ionized gas were derived from the image at 1420 MHz. The electron density and the H II mass were obtained using the expressions of Mezger & Henderson (1967) for a spherical H II region of constant electron density (rms electron density n_e), adopting an electron temperature of 9000 K (Quireza et al. 2006). The derived parameters are listed in Table 4.

The number of UV photons necessary to keep the gas ionized was derived using $N_{Ly-c}(10^{48}\,s^{-1}) = 3.51 \times 10^{-5}\,n_e^2(\mathrm{cm^{-3}})\,\mathrm{R_s^3(pc)}$. Errors in the linear radius, in the rms electron density, and in the number of UV photons come mainly from the distance uncertainty.

Bearing in mind that massive stars have a copious UV flux capable of ionizing the surrounding H I gas, we investigate whether the massive stars in Sh2-173 can provide the energy to ionize the gas. As described in Sect. 1, the only O-type star among the exciting stars is BD+60 39, being the other stars B ones. Given that the number of ionizing photons emitted by an O-type star is significantly larger than that of a B-type star, we neglect the contribution of the UV photons emitted by the stars ALS 6145, 6150, 6155, 6156, 6157, and 6158. The UV photon flux corresponding to an O9V star is in the range N_* ($\mathrm{s^{-1}}$) = (1.1 - 3.6) $\times 10^{48}$ (Vacca, Garmany, & Shull 1996; Martins, Schaerer, & Hillier 2005). By comparing N_* with the UV photons needed to keep the gas ionized (N_{Ly-c}) listed in Table 4, we conclude that the O-type star alone can maintain the H II region ionized.

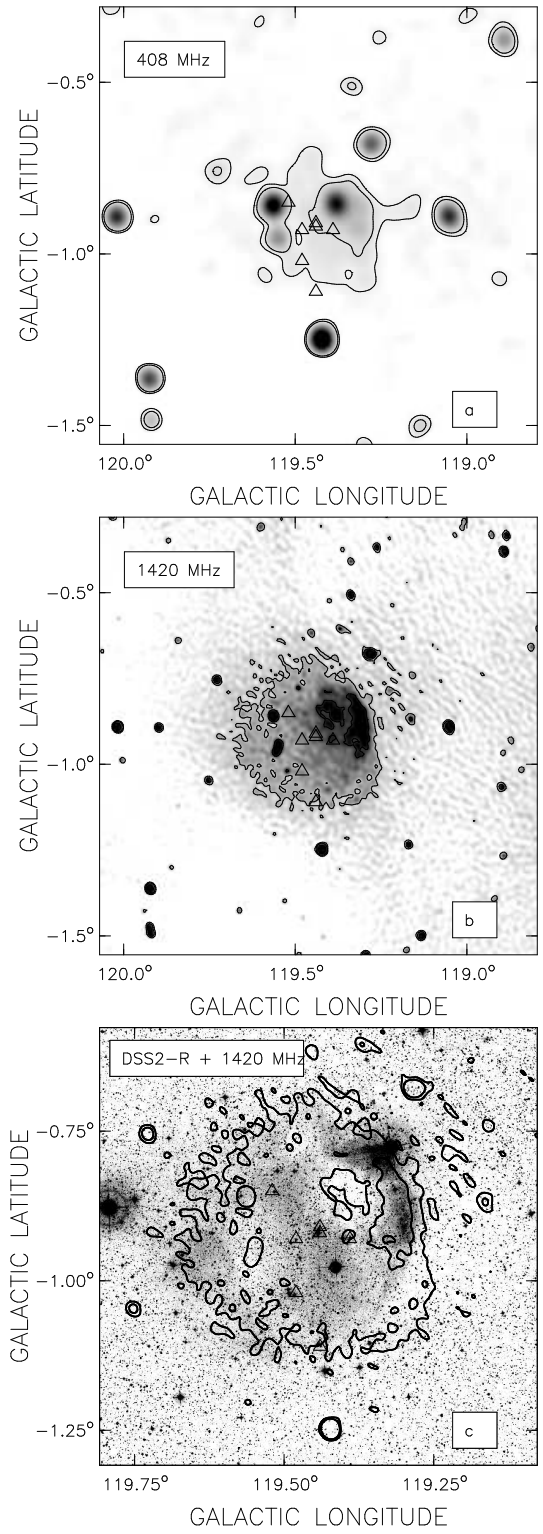


Figure 2. Radio continuum images of the H II region Sh2-173 obtained from the CGPS. The small triangles indicate the position of the OB stars. (*a*) 408 MHz. Contours levels are at 58 and 62 K. (*b*) 1420 MHz. Contour levels are at 5.7 and 6.8 K. (*c*) DSS2-R image (grey-scale) with the 1420 MHz radio continuum contours superimposed. The plotted area is smaller than the one shown in the other images.

Table 4. Main parameters of the observed structures related to Sh2-173.

Adopted distance (kpc)	2.5 ± 0.5	
Ionized gas		
Flux density at 1420 MHz (Jy)	1.8 ± 0.3	
Angular radius (arcmin)	13	
Linear radius (pc)	9.5 ± 2.0	
Ionized mass ($M_\odot$)	480 ± 250	
rms electron density n_e (cm^{-3})	6 ± 1	
Emission measure (pc cm^{-6})	1000 ± 50	
Used Lyman UV photons [N_{Ly-c}] (s^{-1})	$(9.3 \pm 4.0) \times 10^{47}$	
IR emission and dust parameters		
S_{12} (Jy)	50 ± 12	
S_{25} (Jy)	67 ± 30	
S_{60} (Jy)	590 ± 170	
S_{100} (Jy)	1100 ± 500	
L_{IR} ($L_\odot$)	$(9 \pm 4) \times 10^3$	
M_d ($M_\odot$)	1.7 ± 0.7	
T_d (K)	30 ± 5	
H I structure		
Central coordinates	$119.^\circ45$, $-0.^\circ93$	
Angular radius (arcmin)	14	
Linear radius (pc)	10 ± 2	
Velocity interval (v_1, v_2, km s^{-1})	-31.1, -24.6	
Systemic velocity (km s^{-1})	-27.0 ± 1.3	
Expansion velocity (km s^{-1})	5 ± 2	
Velocity width (Δv, km s^{-1})	6 ± 2	
Neutral atomic mass in the shell, M_{sh} ($M_\odot$)	150 ± 100	
Missing atomic mass in the cavity, M_{miss} ($M_\odot$)	120 ± 80	
Molecular clouds	Cloud A	Cloud B
Mean temperature (K)	0.9 ± 0.1	1.2 ± 0.1
Mean area (pc^2)	80	20
Velocity interval (v_1, v_2, km s^{-1})	-38.6, -27.8	-39.4, -34.4
Systemic velocity (km s^{-1})	-32.4 ± 1.0	-36.5 ± 1.0
Mean H_2 column density (10^{21} mol cm^{-2})	1.9 ± 0.6	1.1 ± 0.3
Molecular mass (10^3 $M_\odot$)	5.8 ± 2.0	1.0 ± 0.3
Volume density n_H (cm^{-3})	520 ± 210	560 ± 175

3.2 The Dust

The HIRES IRAS data have been searched for heated dust counterpart to the ionized hydrogen region. Figure 3 shows the 12, 25, 60, and 100 μm images. The image at 12 μm reveals a circular structure which exhibits less emissivity in its central part and is brightest towards lower galactic longitudes. A more diffuse emission distribution is observed at 25 μm. The brightest side at this wavelength coincides with the strongest radio continuum emission. The images at 60 and 100 μm exhibit morphological features similar to those observed at 25 μm. The observed IR morphology and the position of the OB stars suggest that the dust is being heated by the stellar radiation.

The left panel of Fig. 4 exhibits the mid-IR distribution at 8.3 μm (MSX Band A). The image resembles the IR distribution observed at 12 μm. In the right panel a comparison between the IR emission at 8.3 μm (*grey-scale*) and the radio continuum emission at 1420 MHz (*contours*) is shown. Clearly, the IR emission is mostly seen projected outside the continuum emission. The arc feature observed at 8.3 μm is not detected in the other three MSX bands (named C, D, and E). These facts suggest that the polycyclic aromatic hydrocarbons (PAHs) could be the main responsible for the emission detected at 8.3 μm, indicating the existence of a pho-

todissociated region (PDR) in the border of the H II region. The absence of 8.3 μm emission in the interior of the ionized region can be interpreted as the destruction of PAH molecules by the extreme ultraviolet radiation of the ionizing stars. The fact that there is emission detected in the 25 μm IRAS image but not in the MSX E-Band could be due to the lower sensitivity of the MSX instruments.

We include the main IR parameters in Table 4. The IR luminosity L_{IR}, the interstellar dust mass M_d, and the dust temperature T_d were derived assuming a distance D = 2.5 $\pm$ 0.5 kpc. The IR luminosity was estimated following Chan & Fich (1995) as $L_{IR}(L_\odot) = 1.58\, S_{\rm IR}({\rm Jy})\, {\rm D}^2$ (kpc), where S_{IR} is the integrated flux given by $S_{IR} = 1.3(S_{12} + S_{25}) + 0.7(S_{25} + S_{60}) + 0.2(S_{60} + S_{100})$. In order to derive the amount of radiatively heated dust, we have used the equation (Draine 1990) $M_d(M_\odot) = m_n\, S_{60}\; D^2({\rm kpc})\; ({\rm B_n^{5/2}} - 1)$, where $m_n = 0.30 \times 10^{-6}$ g cm^{-2} Hz^{-1} for the adopted value of n ($n = 1.5$) and B_n is the modified Planck function, $B_n = 1.667^{3+n}\; S_{100}/S_{60}$. As for the dust temperature, it was obtained as (Draine 1990) $T_d(K) = (95.94/\ln {\rm B_n})$.

3.3 The neutral hydrogen

As mentioned in Section 1, molecular emission related to Sh2-173 was found at -34.5 km s^{-1} (Blitz et al. 1982), which coincides with the Hα line velocity obtained for the ionized gas, -34.3 ± 0.3 km s^{-1} (Fich et al. 1990). Thus, although the whole H I cube was inspected looking for a structure related to the ionized region, special attention was paid to the velocity interval -34 ± 15 km s^{-1}.

Figure 5*a* shows the mean brightness temperature image within the velocity range -30.3 to -25.4 km s^{-1}. The presence of a small region of low H I emission centered at (*l*, *b*) = (119.°5, $-1.°0$) is evident. This H I void is surrounded by a region of enhanced H I emission. All of the seven stars but one (ALS 6155) listed in Table 1 lie inside the H I minimum. ALS 6155 is seen projected onto the southern border of the cavity. In Figure 5*b*, the 1420 MHz radio continuum image is overlaid in contours for comparison. The positional coincidence is excellent, indicating that the H I feature and the H II region Sh2-173 are quite likely physically related.

A number of parameters characterizing this H I structure can be derived. Given its angular radius of about 14′, we calculate a physical size of 10 $\pm$ 2 pc. The expansion velocity was estimated from the velocity range spanned by the H I feature as $(v_2 - v_1)/2 + 1.3$, where v_1 and v_2 are the minimum and maximum velocities where the structure is observed, and the extra 1.3 km s^{-1} takes into account that the H I caps could be present at $v_1 - 1.3$ km s^{-1} and $v_2 + 1.3$ km s^{-1}. The systemic velocity of the structure corresponds to the velocity where the dimension of the cavity is largest. The mass of the H I ring can be calculated under the assumption of optically thin H I emission. Following the procedure described by Pineault (1998), the H I mass is given by $\rm M_{H\,I}(M_\odot) = 1.3 \times 10^{-3}\, D^2_{kpc}\; \Delta v\, \Omega_{am^2}\, \Delta T_B$, where $\rm D^2_{kpc}$ is the distance to the H I structure and Δv the velocity width over which the H I cavity is detected, in km s^{-1}.

The meaning of Ω_{am^2} and ΔT_B depends on whether we want to find the missing mass in the cavity or the excess mass in the shell. In the first case ΔT_B is the brightness temperature difference between the void and the background, and Ω_{am^2} is the cavity solid angle in arcmin^2. In the second case ΔT_B is the brightness temperature difference between the shell and the background, and Ω_{am^2} is the solid angle of the shell. All the derived parameters are listed in Table 4.

3.4 CO emission distribution

Figure 6 shows the ^{12}CO(1–0) emission distribution within the velocity interval from –27.4 to –40.6 km s^{-1} in steps of 3.3 km s^{-1} (*contours*) overimposed onto the DSS2-R optical image (*grey-scale)*. Each panel is the average of four consecutive CO maps.

In the velocity interval from –27.4 to –30.7 km s^{-1}, the CO emission partially borders the brightest optical emission arc at (*l, b*) $\approx$ (119.°25, –0.°75). In the second velocity interval, from –30.7 to –34.0 km s^{-1}, the CO structure extends towards the south increasing in intensity at lower galactic longitudes. Low molecular arc-shaped emission is distinguished surrounding the optical nebulosity at (*l, b*) $\approx$ (119.°6, –0.°75). The molecular emission distribution in the velocity range from –34.0 to –37.3 km s^{-1} changes in comparison with the previous images. Several different CO features are observed, being the dominant one a CO clump which spatially coincides with the area lacking optical emission at (*l, b*) $\approx$ (119.°4, –0.°85). The fact that radio continuum emission is detected in this region (see Fig. 2b), reinforces the possibility that this molecular clump is the responsible for the observed optical absorption feature. In the last velocity interval, from –37.3 to –40.6 km s^{-1}, the CO structures seen from –27.4 to –34.0 km s^{-1} disappear and most of the CO emission appears projected onto the optical absorption features situated in the central part of the H II region. In two of the velocity channels corresponding to this velocity interval, hardly detected (3 rms) molecular emission is seen projected onto (*l, b*) $\approx$ (119.°57, –1.°0), in coincidence with the other area where optical emission is absent. This CO structure is indicated by a dotted contour in Fig. 6 .

In Fig. 7 the averaged CO emission distribution in the velocity interval from –27.4 to –39.0 km s^{-1} in comparison with the ionized gas, the dust, and the H I distributions in the environs of Sh2-173 is shown. The left panel of Fig. 7 shows the averaged CO emission distribution (*contours*) overimposed onto the DSS2-R optical image (*grey-scale*). There are two main clouds of molecular gas probably related to Sh2-173. Towards lower galactic longitudes, molecular gas partially encircles the H II region (cloud A from here on). The dense molecular gas in this region has probably slowed down the ionization front and the expansion of the H II region in this direction. On the other hand, the area near (*l, b*) = (119.°4, –0.°85), which depicts relatively strong radio emission and is almost free of optical emission, coincides with a cloudlet of molecular material detected within the velocity range from –34.0 to –40.6 km s^{-1} (Cloud B in Fig. 7). This molecular gas and the associated dust should be in front of the ionized material to originate the observed optical absorption. The velocity of cloud B (~ -38 km s^{-1}) is compatible with this material being pushed towards the observer. The difference in radial velocity between cloud A and cloud B allows us to get a rough estimation of the expansion velocity of the molecular gas, which results to be 4 ± 2 km s^{-1}. The middle panel of Fig.7 shows an overlay of the image at 8.3 μm (*grey-scale*) and the CO emission distribution (*contours*). The mid-infrared and molecular emissions present an excellent morphological correspondence. The molecular gas encircles the bright MSX rim. A fainter CO emission feature is observed towards the infrared emission detected at (*l, b*) $\approx$ (119.°6, –0.°75) at 8.3 μm. The right panel of Fig. 7 shows a comparison between the CO and H I emission distributions, showing that the CO structure (cloud A) is lo-

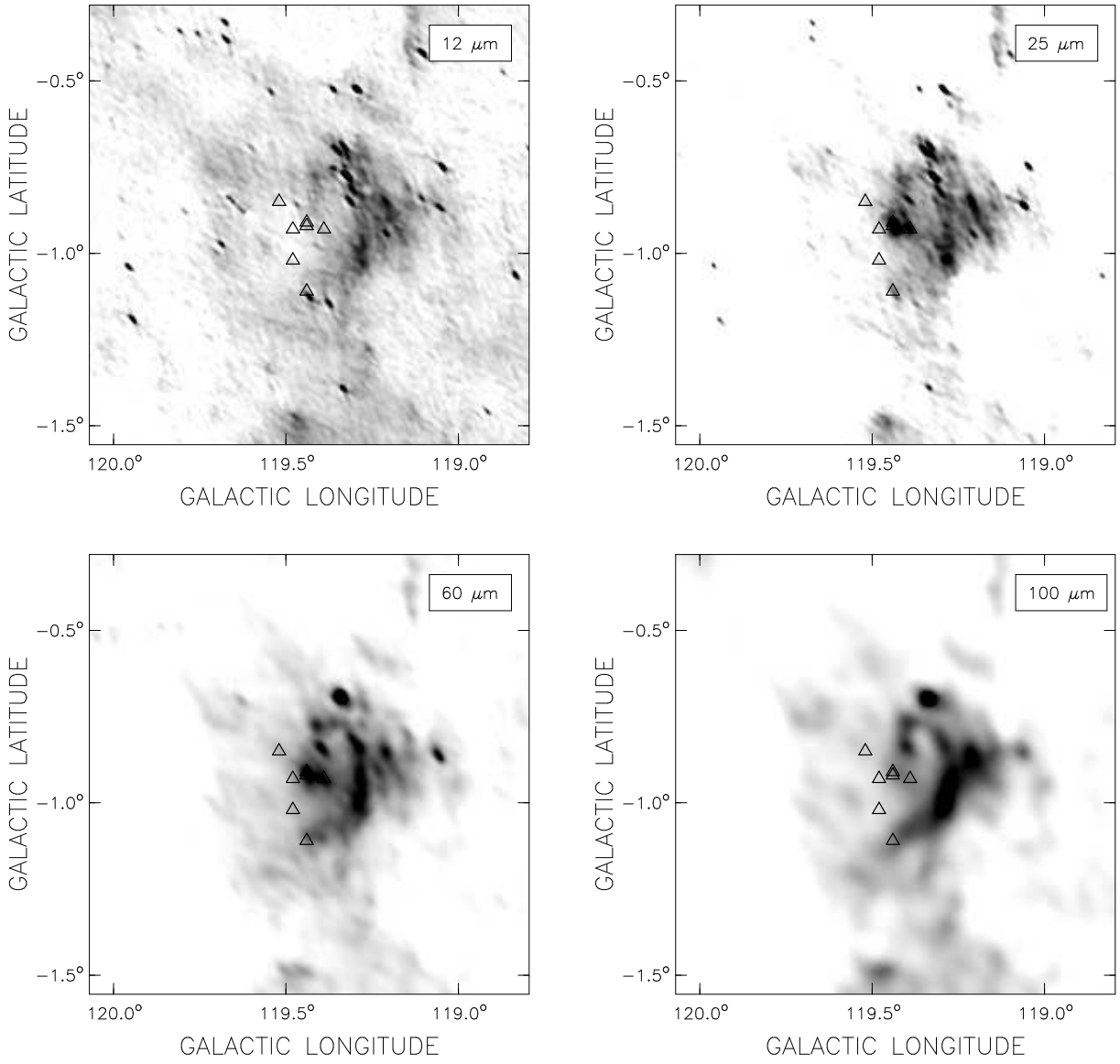


Figure 3. HIRES IRAS maps of the same area as in Fig. 2. The small triangles indicate the position of the seven OB stars listed in Table 1. Grey-scale goes from 3 to 10 MJy sr^{-1} (dark grey) at 12 μm, from 7 to 13 MJy sr^{-1} at 25 μm, from 17 to 55 MJy sr^{-1} at 60 μm, and from 70 to 160 MJy sr^{-1} at 100 μm.

cated slightly further from the ionized gas as compared with the H I shell.

Summing up, the comparison between the spatial distribution of the ionized and neutral gas, together with the dust, reveals a remarkable morphological correspondence. The emission of the ionized gas is partially encircled by an arc shaped feature of mid-infrared emission and an outermost feature of molecular gas. This stratified distribution suggests that the ionization front is bordered by a PDR, detected as the bright rim at 8.3 μm.

Table 4 summarizes the physical parameters of the two molecular clouds shown in Fig. 7 (named cloud A and cloud B) as derived from the ^{12}CO data. The masses were estimated by integrating the CO line intensity as $W_{\rm CO} = \int {\rm T(CO)dv}$, where T(CO) is the average temperature of the molecular gas over the velocity interval where each cloud is observed. To calculate the H_2 column density, the relationship $X = N({\rm H_2})/W_{\rm CO}$ of 1.9×10^{20} cm^{-2}(K kms^{-1})$^{-1}$ (Grenier & Lebrun 1990; Digel, Hunter, & Mukherjee 1995) was considered. The molecular mass was derived from $M[M_\odot] = 4.2 \times 10^{-20} N(H_2) D^2 A$, where D is the distance in pc and A is the solid angle in steradians. Assuming a spherical geometry for both clouds, the volume density

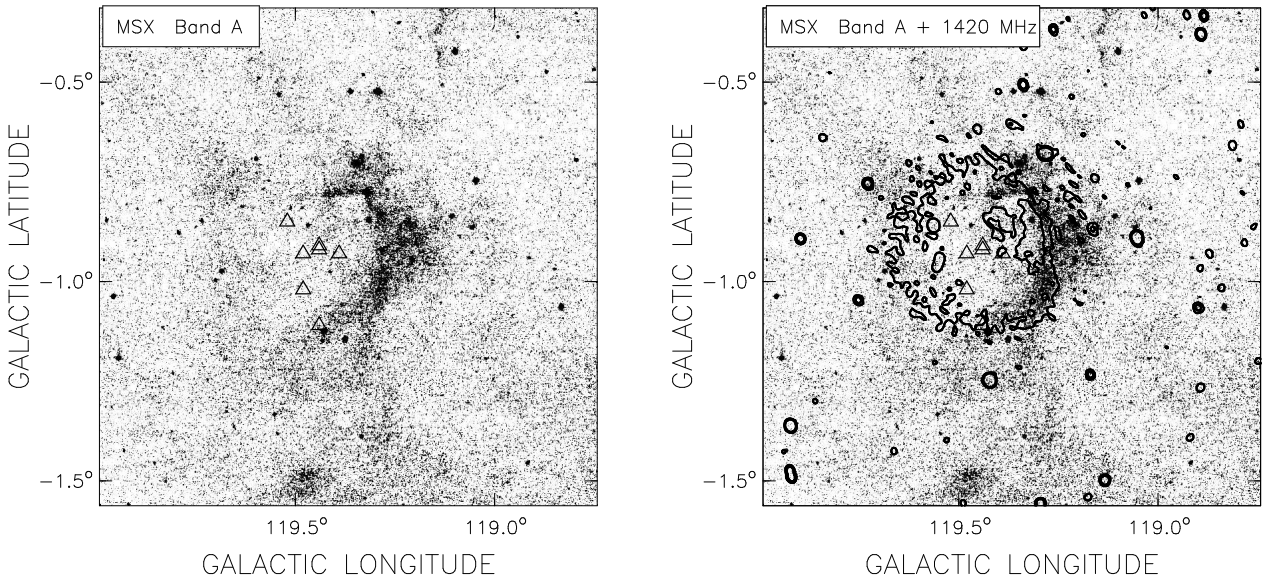


Figure 4. *Left panel*: MSX Band A (8.3 μm) image of the area around Sh2-173. *Right panel*: Overlay of the 8.3 μm image (grey-scale) and 1420 MHz emission (contours). Contour levels are at 6 and 7 K. The small triangles indicate the position of the seven stars listed in Table 1.

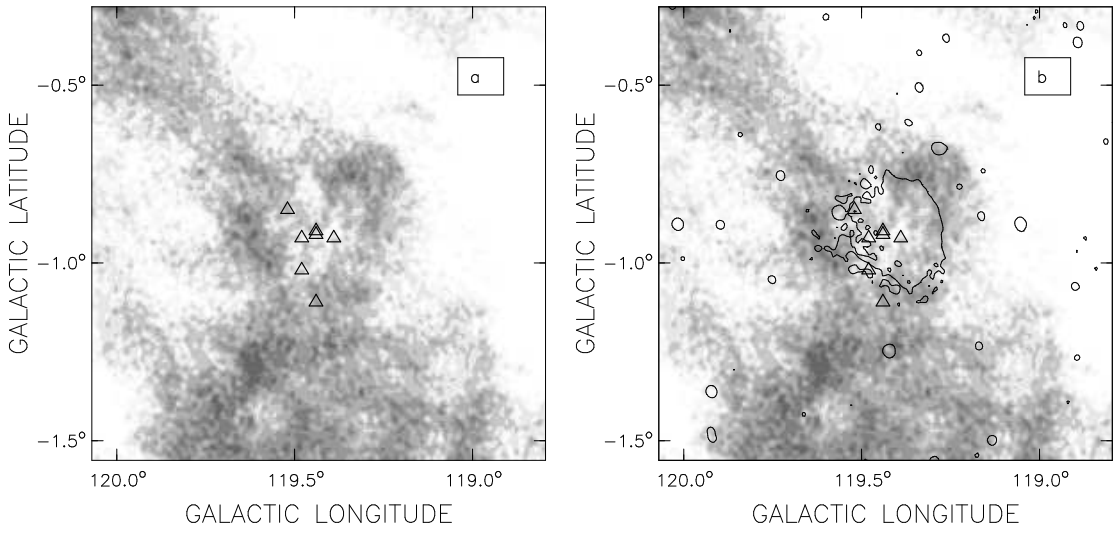


Figure 5. *a*) Averaged H I distribution in the velocity interval -30.3 to -25.4 km s^{-1} showing the H I minimum related to Sh2-173. Grey-scale goes from 35 to 65 K. *b*) Overlay of the averaged H I distribution (grey-scale) and the 6 K radio continuum level at 1420 MHz showing the close correspondence between the H II region and the H I cavity. The small triangles indicate the position of the stars listed in Table 1.

can be estimated as $n = 9.79 \times M[M_\odot]/R^3$, where R is the radius of the molecular cloud in pc.

In order to obtain an estimate of the visual absorption A_V produced by the gas in the direction of Sh2-173, we have used both the H I and CO data cubes. The column densities $N(\mathrm{H\,I})$ and $N(H_2)$ were obtained by integrating the data cubes in the velocity interval from 0 to -40 km s^{-1} in a small box area ($\sim 2'$) over cloud A. The total hydrogen column density was obtained as $N_H = N(\mathrm{H\,I}) + 2\,N(H_2)$. Using the standard conversion factor, the total visual extinction was estimated as $A_V = 5.2 \times 10^{-22}\,N_H$ (Bohlin, Savage, & Drake 1978), which in this case yields $A_V = 4 \pm 1$ mag. For comparison, the visual extinction towards the OB stars listed in Table 1, where no molecular emission is observed, is in the range from 1.3 to 2 mag (Russeil et al. 2007).

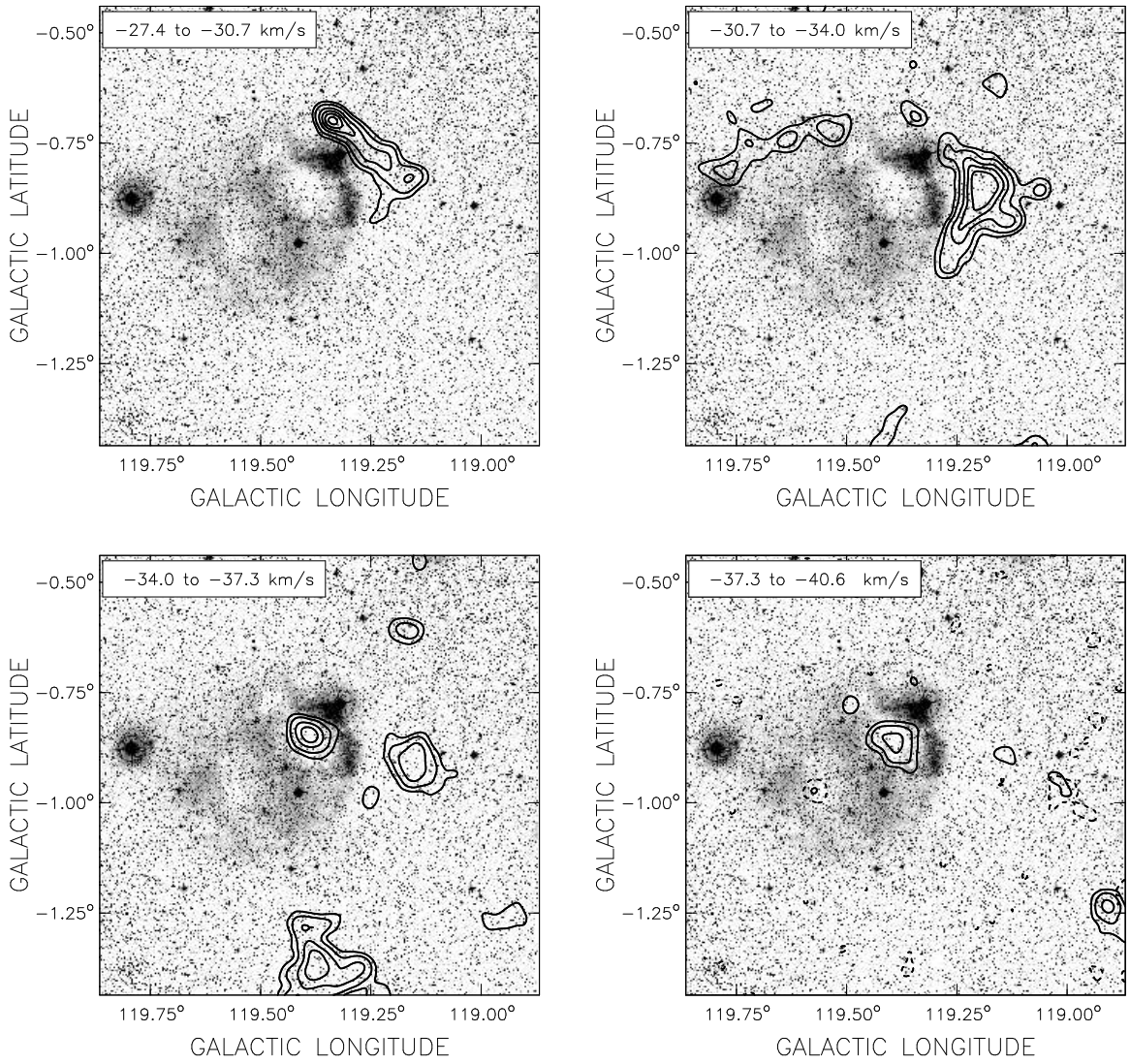


Figure 6. Ionized and molecular gas in the environs of Sh2-173. The images display overlays of the CO emission distribution in the velocity range from –27.4 to –40.6 $\mathrm{km\,s^{-1}}$ (*contours*) and the DSS-R optical image (*grey-scale*). Contour levels are 0.5 K ($\equiv 5\,\sigma$), and from 1 to 5 K in steps of 1 K. Each panel shows the average of four consecutive CO maps. The dotted contour shown in the last velocity interval corresponds to the 0.6 K level of the image at –40.2 $\mathrm{km\,s^{-1}}$.

4 STELLAR FORMATION ACTIVITY

The multiwavelength study of Sh2-173 reveals that it is a classical expanding H II region containing gas and dust, partially encircled by a patchy molecular emission. The interface between the ionized and the molecular gas is clearly evident with the detection of a PDR. The observed morphology leads to the question of whether the expansion of the ionized region could have induced the formation of a new stellar generation in the neighboring molecular envelope. In order to analyze this possibility, we have made a systematic search for young stellar object (YSO) candidates in the area.

To look for primary tracers of stellar formation activity, we used the MSX6C Infrared Point Source Catalogue (Egan et al. 2003) in Bands A (8.3 μm), C (12.1 μm), D (14.7 μm), and E (21.3 μm); the 2MASS All-Sky Point Source Catalogue (Cutri et al. 2003) in bands J (1.25 μm), H (1.65 μm), and K (2.17 μm); and the IRAS Point Source Catalogue [1].

YSO candidates were searched in a $1^\circ \times 1^\circ$ box area centered at (l, b) = ($119\overset{\circ}{.}36$, $-0\overset{\circ}{.}9$). A total of 30 IRAS point sources were found projected onto the analyzed region. Junkes, Fürst, & Reich (1992)'s conditions for YSOs are: $S_{100} \geqslant 20$ Jy, $1.2 \leqslant \frac{S_{100}}{S_{60}} \leqslant 6.0$, $\frac{S_{60}}{S_{25}} \geqslant 1$, and Q_{60}+$Q_{100} \geqslant 4$, where S_λ and Q_λ are the flux density and the quality of the IRAS flux in each of the observed bands, respectively. Only 2 of the 30 observed IRAS sources fulfill these conditions and may be classified as protostellar candidates.

The MSX sources were classified based on the Lumsden et al. (2002)'s criteria. The selection of the sources is made taking into account their loci in the (F_{21}/F_8, F_{14}/F_{12}) diagram, where F_λ

[1] 1986 IRAS catalogue of Point Sources, Version 2.0 (II/125)

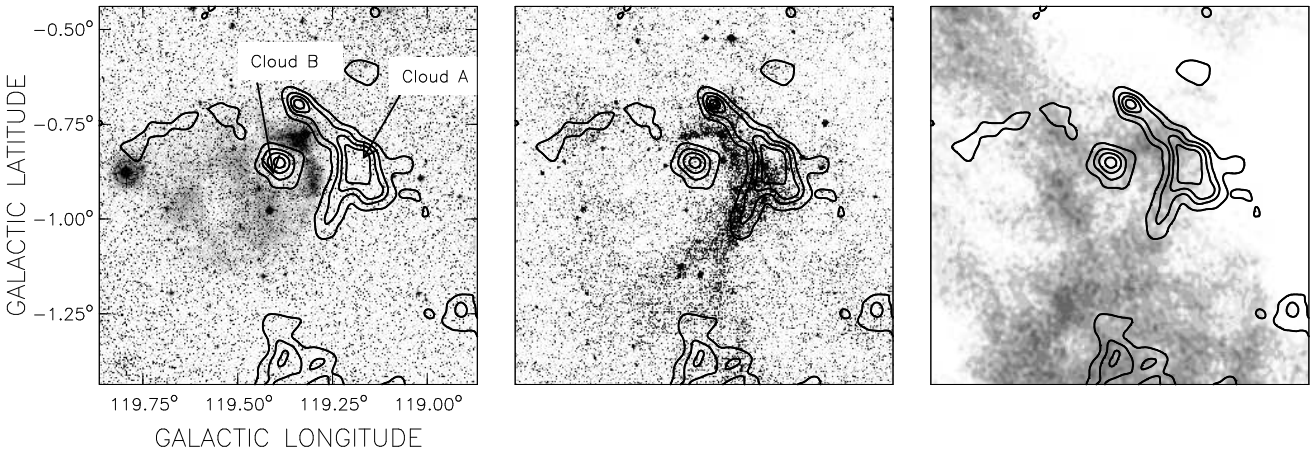


Figure 7. Dust and gas in the environs of Sh2-173. In the three panels the contours show the CO emission distribution within the velocity range from –27.4 to –39.0 $\mathrm{km\,s^{-1}}$. Contour levels are from 0.2 to 1.8 in steps of 0.4 K. *Left panel*: The CO contours are superimposed on the DSS2-R optical image (*grey-scale*). *Middle panel*: The CO contours are superimposed on the MSX Band A image. *Right panel*: The CO contours are superimposed on the averaged H I distribution.

denotes the flux in each band. According to these criteria, massive young stellar object (MYSO) candidates have $F_{21}/F_8 \gtrsim 2$ and $F_{14}/F_{12} \gtrsim 1$, while compact HII regions (CH II) present $F_{21}/F_8 \gtrsim 2$ and $F_{14}/F_{12} < 1$. Evolved stars occupy the region where $F_{21}/F_8 \leqslant 2$ and $F_{14}/F_{12} \leqslant 1$. We have found 40 MSX sources projected onto the area, however neither of them satisfy the criteria to be classified as a MYSO nor a CH II.

To look for tracers of stellar formation activity in the 2MASS catalogue, we have adopted the criteria developed by Kerton et al. (2008). Based on a sample of YSOs having low ($< 2\ M_\odot$) and intermediate ($2 < M_\odot < 9$) masses extracted from Kenyon & Hartmann (1995) (T Tauri) and Thé, de Winter, & Perez (1994) (Herbig/AeBe), respectively, Kerton et al. (2008) inferred a colour criteria to analyze the presence of stellar formation activity in the surroundings of the H II region KR 140. They scaled the data of the sample to the distance of KR 140 (2.3 kpc) and the corresponding visual extinction (A_v = 5.5 mag). Using the 2MASS Point Source Catalogue, and taking into account different photometric qualities and the adopted colour criteria, these authors divided the YSO candidates in four groups, named P1, P1+, P2, and P3. P1 and P1+ sources have the best photometric quality (ph_qual = A, B, C, or D). P1 sources lie below the reddening vector associated with an O6 V star, while P1+ sources lie in the overlapping region of T Tauri and main sequence stars. The P2 group contains sources which have not been detected in the J-band (ph_qual = U in this band). In this case, the adopted J-magnitude is a lower limit and consequently the corresponding value of (J-H) is a lower limit as well. Thus, the actual position of the P2 sources in the (J-H)-axes is likely to be towards higher (J-H) values. Finally, the sources belonging to the P3 group have J and H magnitudes that are lower limits, so their colour (J-H) can not be considered. These sources can not be included in the CC diagram, and their real position on the CM diagram may be towards higher values of (H-K). To analyze the presence of 2MASS YSO candidates in the surroundings of Sh2-173 we have adopted the Kerton et al.'s criteria scaled to the distance adopted for Sh2-173 (2.5 kpc) and the visual absorption in this direction (A_v = 4.0 mag). The modified criteria are listed in Table 5.

Table 5. Selection criteria for 2MASS YSO candidates.

Classification	Colour criteria
P1	$(J-H) > 0.835$ $(J-H) < 1.7\,(H-K) - 0.087$
P1+	$1.135 < (J-H) < 1.435$ $(J-H) > 1.7\,(H-K) - 0.087$ $(J-H) < 1.7\,(H-K) + 0.3685$ $K > 14.5$
P2	$(J-H)_L < 1.7\,(H-K) - 0.087$ $(H-K) > 0.91$
P3	$(H-K)_L > 0.91$

The underscript "L" indicates a lower limit.

A total of 23988, 135, and 134 sources from the 2MASS catalogue were examined in order to find *P1* or *P1+*, *P2*, and *P3* candidates, respectively. From the 23988 sources, only 81 and 10 were classified as *P1* and *P1 +*, respectively. Out of the 135 candidates, 19 were identified as *P2* sources, while only 5 out of the 134 candidates were classified as *P3* sources. Thus, a total of 115 2MASS sources were found to be YSO candidates. However, 2 of these sources had to be excluded from the sample since they were identified as part of the galactic contamination in the 2MASS catalogue (i.e. galcontam=2). Figure 8 shows the CC (top panel) and CM (bottom panel) diagrams for the YSO candidates projected onto the molecular gas associated with Sh2-173. The CM diagram also shows the position of the Sh2-173's exciting stars. The reddening vectors for an early type (O9 V) and a late-type (M0 III) stars (Tokunaga 2000) are represented by two parallel lines in the CC diagram using extinction values from Rieke & Lebofsky (1985). For the location of the main sequence we have used for the O-stars the values given by Martins & Plez (2006), and for the

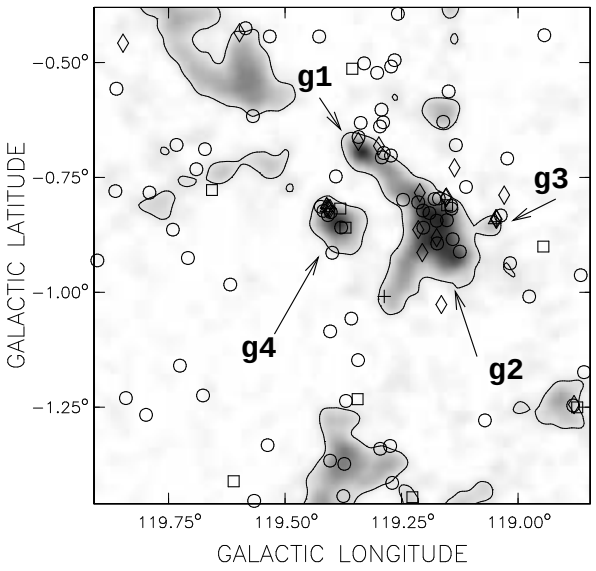


Figure 9. Infrared point sources classified as YSO candidates overlaid onto the CO distribution averaged between the velocity range from –27.4 to –49.8 $\mathrm{km\,s^{-1}}$. IRAS, P1, P1+, P2, and P3 sources are indicated as crosses, circles, squares, diamonds, and triangles, respectively. The locations of the four groups, g1, g2, g3, and g4, described in the text are indicated.

late-type stars (B to M) the ones given by Tokunaga (2000) and Drilling & Landolt (2000). The main sequence obtained for a distance of 2.5 kpc is indicated by filled diamonds in the CM diagram. The location of the YSO candidates in the CC diagram is in concordance with the numerical models developed by Robitaille et al. (2006).

Figure 9 shows the location of the YSO candidates with respect to the ^{12}CO emission distribution in the velocity range from –27.4 to –49.8 $\mathrm{km\,s^{-1}}$. IRAS, P1, P1+, P2, and P3 sources are indicated as crosses, squares, circles, diamonds, and plus signs, respectively. As can be inferred from the figure, 65 of the 115 YSO candidates appear projected onto molecular gas, from which 46 are located onto molecular clouds probably related to Sh2-173 (clouds A and B). There is a clear concentration of sources towards the brightest parts of the CO emission associated with Sh2-173. Based on their relative location, we have separated them into four groups: g1, g2, g3, and g4 (see Fig. 9). The groups g1 and g2 contain 8 and 20 2MASS sources, respectively, and are located in the periphery of the optical nebula, onto the PDR. The group g3 is conformed by sources located towards lower galactic longitudes, onto cloud A. The sources of the group g4 are located onto cloud B.

The main data of the IRAS and 2MASS sources that are seen projected onto molecular gas are listed in Table 6. It is worth mentioning that an inspection of the CO data cube reveals that there is only one velocity component in the direction of Sh2-173. This fact strongly suggests that the YSO candidates suffer from extinction due to the molecular material related to Sh2-173.

To sum up, based on different infrared colour criteria and on the location of the molecular emission, we have identified 46 YSO candidates probably associated with Sh2-173.

The presence of a PDR is a clear proof of the interaction between the H II region and the molecular gas, since it is a region directly affected by the expansion of the ionized gas and by the UV photons of the exciting stars. Thus, the relative location of the YSO candidates with respect to the PDR may be considered as an indication of the role that the H II region is playing in the formation of the new stars. The probability for a source of being triggered by the action of the H II region is higher when it is located inside the region of direct influence of the H II region (Kerton et al. 2008, and references therein).

Figure 9 shows that there are two groups of sources, named g1 and g2, located adjacent to the PDR, while the group g3 is located further, towards lower galactic longitudes. The possibility for the group g4 of being located near or onto a PDR can not be discarted. A face-on PDR, which could not be detected, may be present between the ionized region and the molegular gas.

5 THE BIG PICTURE

As mentioned in Section 1, Sh2-173 lies in the border of a large H I shell observed in the Perseus arm (Fich 1986; Moór & Kiss 2003). Using CGPS data (Taylor et al. 2003), we have inspected the area looking for the H I structure observed by Fich (1986) using low resolution data.

An inspection of the whole data cube reveals the presence of an H I minimum which is first seen near -20 $\mathrm{km\,s^{-1}}$ and which can be followed up to -50 $\mathrm{km\,s^{-1}}$. Figure 10 shows the H I distribution averaged in the velocity range from –20 to –50 $\mathrm{km\,s^{-1}}$, where the large H I cavity is evident centred at (*l*, *b*) = (117.°8, +1.°5), as well as the H I shell encircling it. Following the standard nomenclature for galactic shells, we designate this structure as GSH 117.8+1.5-35.

Along the mentioned velocity range, both the H I minimum and the H I shell are well defined as a large structure, although, as in many other H I shells, the typical behavior of an expanding structure (i.e. a ring that start as a cap, reach its greatest angular dimension at the systemic velocity and then shrink back to a cap) is not completely observed. In this case the receding cap is missing, while the approaching cap is detected, at about –50 $\mathrm{km\,s^{-1}}$. The absence of the receding cap could be due to confusion effects. Other possible explanation is that the receding part may be expanding into a lower density medium, as it would happen if for example it were located near the border of the Perseus arm. On the other hand, as expected when dealing with high resolution H I data, there are several small-scale structures inside and around the large ring. These smaller H I features change in shape and size along the velocity range where the large shell is defined, and are possibly related to the individual action of every massive star present in the area. In this paper we will just focus on the large scale structure.

The location of the stars belonging to Cas OB5 (Garmany & Stencel 1992) are indicated in Fig. 10, showing that most of them lie outside the large H I minimum. Particularly, two O-stars belonging to Cas OB5 are seen projected towards a smaller H I minimum centred at (*l*, *b*) = (117.°3, -1.°3). The position of the WN4 star (WR 159) (Negueruela 2003) is indicated with a larger circle.

In Figure 11 a 1420 MHz radio continuum image of the same area displayed in Fig. 10 is shown. The ellipse delineates the location of the H I shell. A minimum in the radio continuum emission in coincidence with the H I cavity is observed, although the presence of two SNR (CTB 1 and G116.5+1.1) makes it less evident. Several Sharpless H II regions are projected onto the thick H I shell, being Sh2-173 one of them. Based on Hα observations, Fich et al. (1990)

Table 6. YSO candidates projected onto the molecular clouds A and B.

IRAS sources								
#	Designation	(l, b)	Fluxes [Jy]				L_{IRAS}[$L_\odot$]	Group
			12 μm	25 μm	60 μm	100 μm	For D = 2.5 kpc	
1	00158+6128	119.°057 –0.°87	0.92	2.29	8.78	23.29	$\sim$ 180	g3
2	00179+6121	119.°282 –1.°02	0.32	0.3	5.89	23.89	$\sim$ 110	-
2MASS sources								
#	Designation	(l, b)	J	H	K	$(H-K)$	$(J-H)$	Group
P1								
3	00183077+6145567	119.°047 –0.°857	14.317	13.132	12.041	1.091	1.185	g3
4	00211376+6146520	119.°368 –0.°881	16.892	15.932	15.317	0.615	0.96	g4
5	00193852+6143342	119.°175 –0.°913	16.816	15.858	15.07	0.788	0.958	g2
6	00194881+6147427	119.°204 –0.°847	15.799	14.91	14.322	0.588	0.889	g2
7	00202395+6154406	119.°286 –0.°740	17.227	16.246	15.499	0.747	0.981	g1
8	00201448+6154455	119.°268 –0.°736	16.76	15.899	15.007	0.892	0.861	g1
9	00212578+6143577	119.°386 –0.°932	16.827	15.967	15.356	0.611	0.86	g4
10	00191976+6147310	119.°146 –0.°843	16.041	15.104	14.472	0.632	0.937	g2
11	00212969+6149057	119.°404 –0.°848	17.11	16.16	15.359	0.801	0.95	g4
12	00193126+6148555	119.°172 –0.°823	16.706	15.822	14.851	0.971	0.884	g2
13	00192242+6143509	119.°144 –0.°904	16.382	15.458	14.68	0.778	0.924	g2
14	00191965+6147518	119.°147 –0.°837	16.709	14.76	13.56	1.2	1.949	g2
15	00202211+6158243	119.°290 –0.°678	16.455	15.518	14.651	0.867	0.937	g1
16	00193625+6146178	119.°176 –0.°867	16.28	15.413	14.767	0.646	0.867	g2
17	00204518+6157266	119.°333 –0.°699	14.873	13.387	12.373	1.014	1.486	g1
18	00195258+6148460	119.°213 –0.°830	16.51	15.633	14.967	0.666	0.877	g2
19	00212565+6148318	119.°395 –0.°856	16.559	15.339	14.464	0.875	1.22	g4
20	00195062+6145397	119.°203 –0.°881	15.993	15.072	14.361	0.711	0.921	g2
21	00194259+6147191	119.°191 –0.°852	16.584	15.694	14.876	0.818	0.89	g2
22	00192579+6146125	119.°156 –0.°866	15.701	14.751	14.115	0.636	0.95	g2
23	00213187+6149382	119.°409 –0.°839	16.106	14.707	13.742	0.965	1.399	g4
24	00212247+6148506	119.°389 –0.°850	16.616	15.265	14.375	0.89	1.351	g4
25	00204129+6159065	119.°329 –0.°671	16.997	16.016	15.358	0.658	0.981	g1
26	00193569+6148554	119.°180 –0.°824	16.703	15.597	14.857	0.74	1.106	g2
27	00191679+6142153	119.°130 –0.°929	16.654	15.789	15.092	0.697	0.865	g2
28	00202147+6155100	119.°282 –0.°731	16.356	15.48	14.887	0.593	0.876	g1
P1+								
29	00210933+6146474	119.°359 –0.°881	16.811	15.655	15.132	0.523	1.156	g4
30	00192372+6147592	119.°155 –0.°836	16.992	15.674	15.015	0.659	1.318	g2
31	00211236+6149088	119.°370 –0.°843	16.609	15.287	14.684	0.603	1.322	g4
P2								
32	00182469+6148202	119.°041 –0.°816	>16.575	16.038	15.026	1.012	>0.537	g3
33	00192419+6148555	119.°158 –0.°821	>17.416	15.415	13.609	1.805	>2.001	g2
34	00193839+6144163	119.°176 –0.°901	>16.996	15.743	14.791	0.952	>1.253	g2
35	00212409+6149210	119.°393 –0.°842	>16.361	16.017	14.359	1.657	>0.344	g4
36	00202552+6156054	119.°292 –0.°717	>16.886	15.338	14.119	1.219	>1.549	g1
37	00192337+6148577	119.°156 –0.°820	>17.844	15.739	14.21	1.529	>2.106	g2
38	00212265+6149170	119.°390 –0.°843	>16.938	15.862	14.888	0.973	>1.077	g4
39	00204593+6156560	119.°334 –0.°708	>16.118	15.215	13.961	1.255	>0.902	g1
40	00212591+6149307	119.°397 –0.°840	>14.951	15.553	14.619	0.934	>0.601	g4
41	00195601+6145301	119.°213 –0.°885	>16.325	15.866	14.965	0.901	>0.458	g2
42	00195468+6142421	119.°205 –0.°931	>17.000	15.968	15.0559	0.913	>1.032	g2
43	00194992+6149530	119.°210 –0.°811	>15.847	15.501	14.439	1.063	>0.346	g2
P3								
44	00183752+6145299	119.°060 –0.°866	>18.312	>16.298	15.008	>1.29	-	g3
45	00212628+6149244	119.°397 –0.°842	>18.274	>16.110	14.022	>2.087	-	g4
46	00212574+6149479	119.°397 –0.°835	>18.1310	>16.170	14.404	>1.766	-	g4

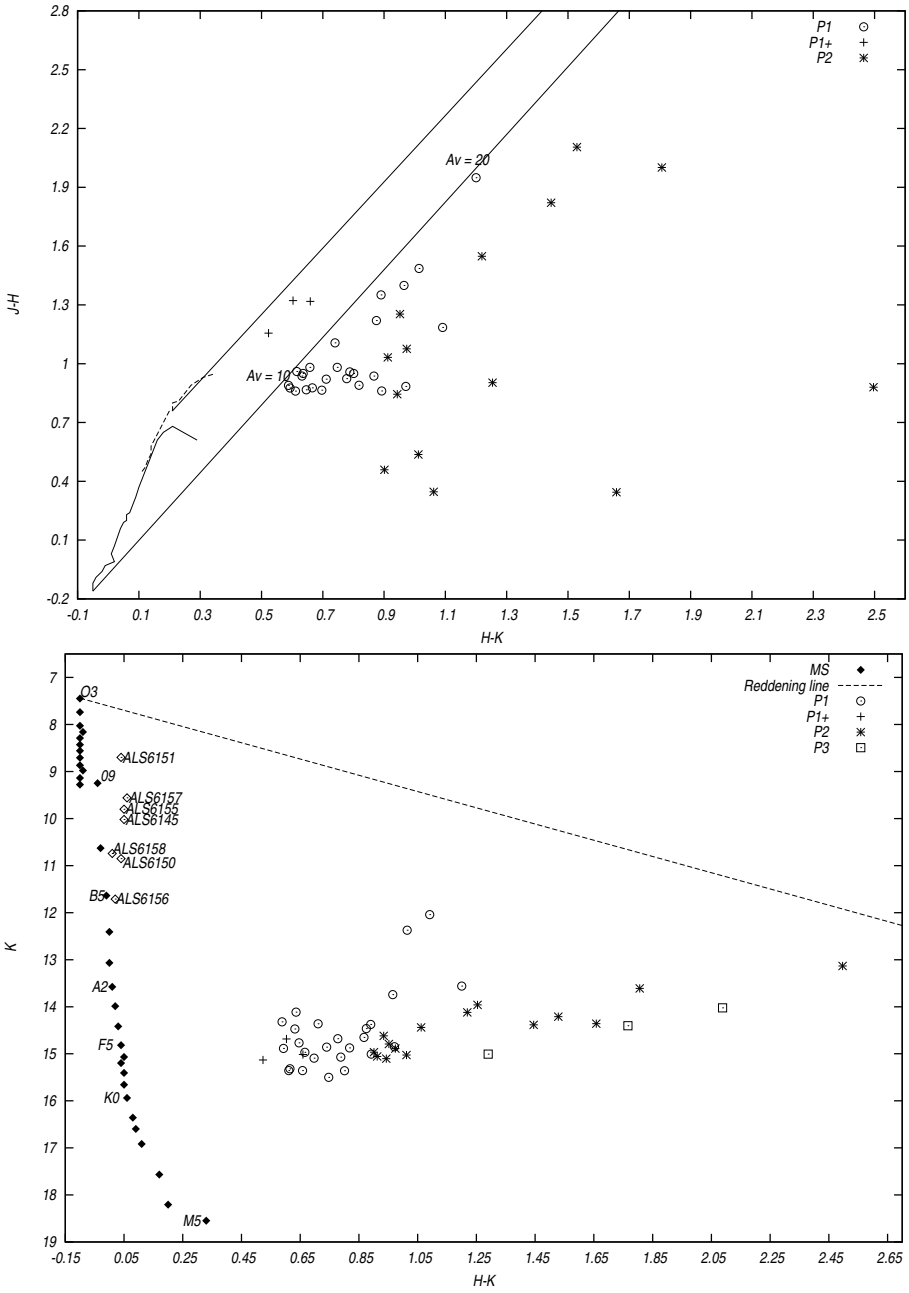


Figure 8. CC and CM diagrams of the 2MASS YSO candidates projected onto clouds A and B. P1, P1+, P2, and P3 sources are indicated by circles, crosses, asterisks, and squares, respectively. *Upper panel*: $(H-K, J-H)$ diagram. The positions of the derredened early-type main sequence and giant stars are shown. The reddening curves for MO III stars (upper line) and O9 V stars (lower line) are indicated. The colours $(J-H)$ corresponding to P2 sources are lower limits. *Lower panel*: $(H-K, K)$ diagram. The position of the main sequence (Tokunaga 2000; Drilling & Landolt 2000; Martins & Plez 2006) with $\mathrm{A_v} = 4$ mag at a distance of 2.5 kpc is indicated by filled diamonds. The locations of the OB stars related to Sh2-173 are indicated by their corresponding names. The reddening curve for an O3 star is shown with a dashed line. The colours $(H-K)$ corresponding to P3 sources are lower limits.

derived the radial velocity of galactic H II regions. From their work, we found out that most of the H II regions shown in Fig. 11 have a radial velocity between –32 and –55 $\mathrm{km\,s^{-1}}$, in coincidence with the radial velocity in which the large H I shell is detected. Only two regions, Sh2-171 and Sh2-167, have radial velocities outside this range, of about $-12\ \mathrm{km\,s^{-1}}$ and $-66\ \mathrm{km\,s^{-1}}$, respectively. As mentioned by Cazzolato & Pineault (2003), Sh2-180, Sh2-181, and Sh2-182, may be associated with Cas OB7. Sh2-179 is a planetary nebula (Kerber et al. 2003). Besides the H II regions, four SNR are seen projected in the area, G114.3+0.3, G116.5+1.1, CTB 1, and G120.2+01.4 (Tycho).

The HIRES 60 μm image of the same area is shown in Fig. 12. The large-scale structure is similar to the infrared loop GIRL G117+00 shown by Kiss et al. (2004). The infrared emission shows a distribution similar to the radio continuum one. A minimum in the 60 μm emission is evident inside the large H I shell (indicated by the ellipse). One of the main differences between this image and the one shown in Fig. 11 is the absence of SNRs at infrared

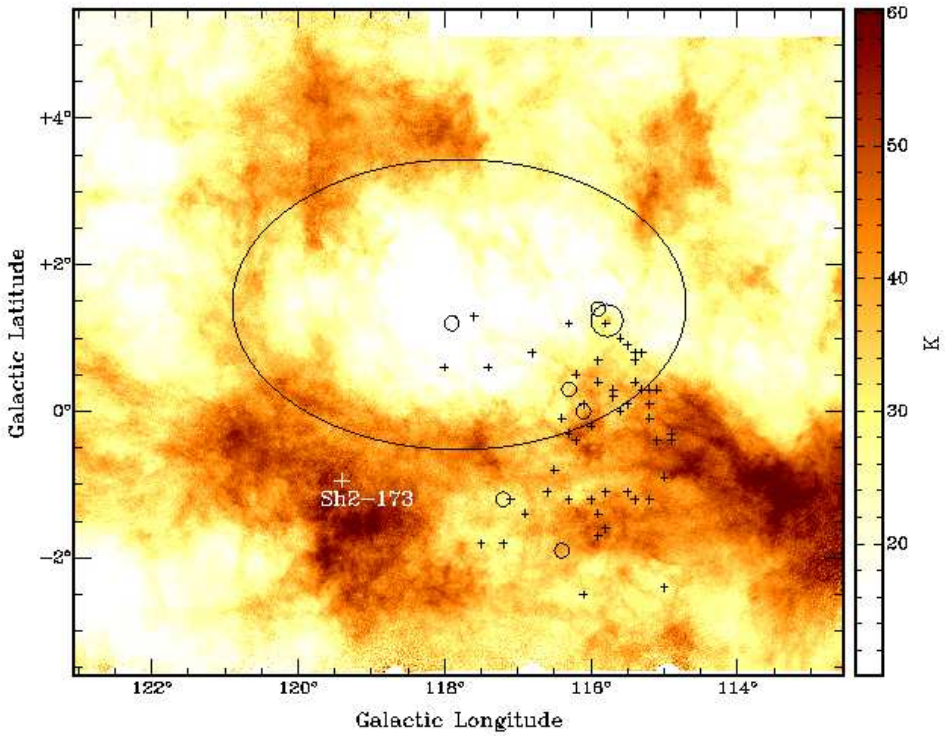


Figure 10. Averaged H I emission distribution between the velocity range from –50 to –20 $\mathrm{km\,s^{-1}}$. The circles and crosses indicate the position of the stars belonging to Cas OB5 according to Garmany & Stencel (1992). The small circles correspond to O-type stars, while crosses mark the location of B stars. The large circle indicates the position of WR 159. The ellipse delineates the location of the H I shell.

wavelengths. As expected, the infrared emission associated with H II regions is clearly observed.

Figure 13 shows the averaged CO emission distribution in the velocity range from –50 to –20 $\mathrm{km\,s^{-1}}$. The CO data were obtained from the Five College Radio Astronomical Observatory (FCRAO) CO Survey. The image reveals several molecular clouds sparsely located at the shell's border.

It is generally believed that expanding supershells may trigger star formation at their edges. As the shell expands, it becomes gravitationally unstable, providing a physical mechanism to form clouds and induce star formation along its periphery (e.g. McCray & Kafatos 1987; Elmegreen 1998). There are some observational evidence confirming the importance of the shell's evolution in creating new stars. Patel et al. (1998) analyzed the origin and evolution of the Cepheus bubble and concluded that the Cep OB2 association was probably triggered by the action of an earlier generation of massive stars and suggested that a third generation of stars has recently formed as a consequence of the evolution of the shell. Oey et al. (2005) analyzed the W3/W4 Galactic star forming complex and suggested that it consists of a hierarchical system of three generations: a supergiant shell triggered the formation of IC 1795 in W3, which in turn triggered the star formation in its surroundings. They confirmed this scenario based on the age sequence showed for the different generations. Arnal & Corti (2007) found a new H I supershell (GS263-02+45) which has the OB-association Bochum 7 located in its border. They concluded that the association may have been born as a consequence of the evolution of GS263-02+45.

In our case, having in mind the scenario previously described, i.e. a large expanding H I shell containing several H II regions in its edge, and where at least one of them, Sh2-173, shows evidence of star forming processes taking place in its surrounding molecular material (see Section 4), we wonder if this could be other case of a hierarchical system of three generations. If this were the case, it should be reflected by a corresponding age sequence. In what follows we will briefly discuss possible age estimates for both, the H II region Sh2-173 and the large H I shell GSH 117.8+1.5-35.

Given that the main exciting star of Sh2-173 is still visible, an upper limit for its age can be estimated. The main-sequence lifetime for an O9 star is about 5.0 Myr (Schaerer & de Koter 1997). On the other hand, a lower limit to the age can be estimated considering the sound crossing time, R/v_s, where v_s is the sound speed in the ionized gas ($\sim 15\ \mathrm{km\,s^{-1}}$) and R is the radius of the H II region. For Sh2-173 the corresponding lower limit is about 0.6 Myr. As a different approach, the age of the H II region can be inferred using the simple model described by Dyson & Williams (1980) for an expanding ionized region in a uniform medium. The expansion of an H II region is highly dependent on the density of the surrounding gas. As a rough estimate, the original ambient density can be obtained by distributing the total mass related to the structure (ionized, neutral atomic, and molecular) over a sphere of 12 ± 2 pc in radius, which yields $n_o = 41 \pm 25\ \mathrm{cm^{-3}}$. Under these condi-

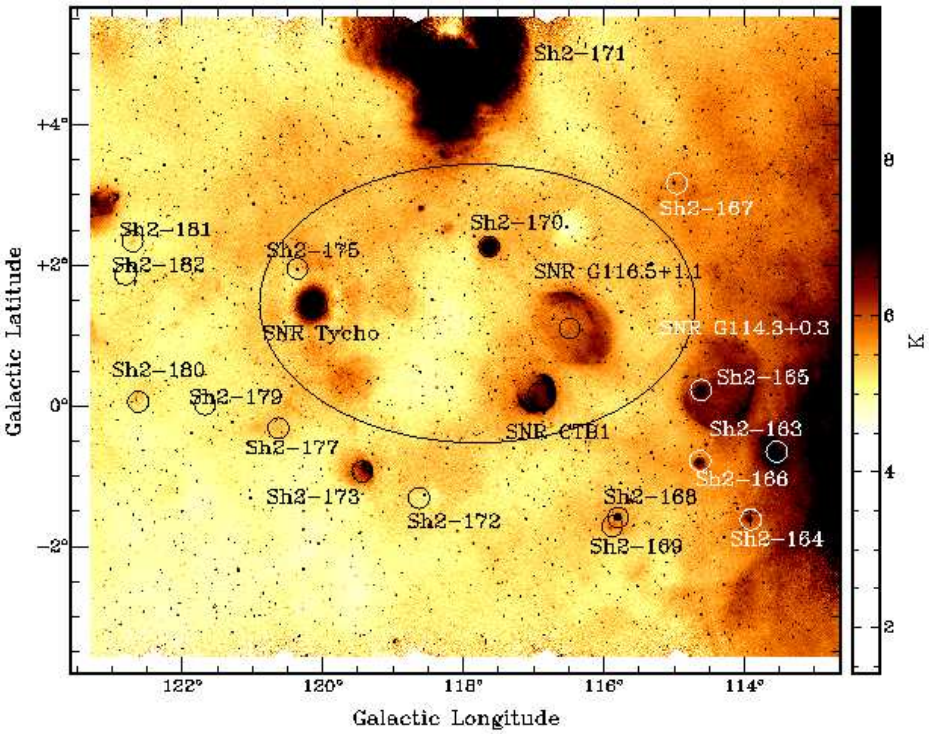


Figure 11. 1420 MHz radio continuum image from the CGPS survey. The ellipse delineates the H I shell shown in Fig.10. The location of the Sharpless H II regions and the SNRs present in the area are indicated by circles.

tions, we can infer that the H II region has been expanding during 0.1 - 1.0 Myr. This range for the dynamical age, together with the age limits estimated above, suggest that the age of Sh2-173 could be between 0.6 and 1.0 Myr. Using the same simple model the expansion velocity of the H II region can be inferred. We obtained $V_{\rm exp} = 6 \pm 3$ km s^{-1}, which is in agreement with the expansion velocity estimated for the molecular gas (4 ± 2 km s^{-1}). Thus, the ionized and molecular gas are expanding at the same velocity, as expected according to the models of Hosokawa & Inutsuka (2006) when the molecular material has been accumulated behind the ionization front.

A rough estimate for the age of the large H I shell, GSH 117.8+1.5-35 , can be obtained using a simple model to describe the expansion of a shell created by a continuous injection of mechanical energy (Weaver et al. 1977). In this way, the dynamical age of the H I structure can be estimated as $t_{\rm dyn} = 0.6\,R$ (pc)$/V_{\rm exp}$(km s^{-1}), where R is the radius of the shell and $V_{\rm exp}$ the expansion velocity. The expansion velocity can be obtained as $V_{\rm exp} = (v_2 - v_1)/2 + 1.3$ km s^{-1} (see Section 3.3). Given that the large H I shell is observed over some 30 km s^{-1}, an expansion velocity of about 16 km s^{-1} is inferred. Thus, considering $R = 135 \pm 20$ pc (for a distance of 2 kpc, see the discussion below) and $V_{\rm exp} = 16 \pm 2$ km s^{-1}, an age of 5 ± 1 Myr is obtained, which is large as compared with the age estimate obtained for Sh2-173.

Concerning the origin of the large shell, Fich (1986) suggested that the three supernova remnants located within the H I shell have actively enlarged it, which was presumably previously created by the joined action of several stellar winds and/or several supernova remnants. Based on the location of Cas OB5 on the sky, Moór & Kiss (2003) associated the expanding shell with the OB association. However, an energetic analysis has not been made in order to test this possibility. Are the massive stars (O-type stars) belonging to Cas OB5 capable of creating such a shell?. The first condition that should be checked is if the H I shell and Cas OB5 are at comparable distances from the Sun. The systemic velocity adopted for the large shell is -35 km s^{-1}, while according to Humphreys (1976), Cas OB5 has $V_{\rm LSR} = -39.5$ km s^{-1}. On the other hand, Garmany & Stencel (1992) determined for Cas OB5 a distance modulus of DM = 11.5 mag, which yields a distance D = 2 kpc. As mentioned in Section 1, the presence of non-circular motions in the Perseus arm is important and should be taken into account. An inspection of the *observed* radial velocity field of the Galaxy derived by Brand & Blitz (1993) gives for the adopted systemic velocity a distance of about 1.8-2 kpc. Thus, we will consider a distance of 2 kpc for Cas OB5 and the H I shell.

A second condition that should be checked is if the energy budget of the massive stars is enough to create the large shell. The mechanical energy output of the stars should be compared with the kinetical energy of the shell. As can be seen in Fig. 10, four O-type stars (BD+62 2299 (O8), BD+61 2550 (O9.5II), BD+61 2559 (O9V), and HD 108 (O5 f)) and one Wolf-Rayet star (WR 159 (WN4)) are seen projected inside the large H I minimum. All these massive stars are supposed to belong to

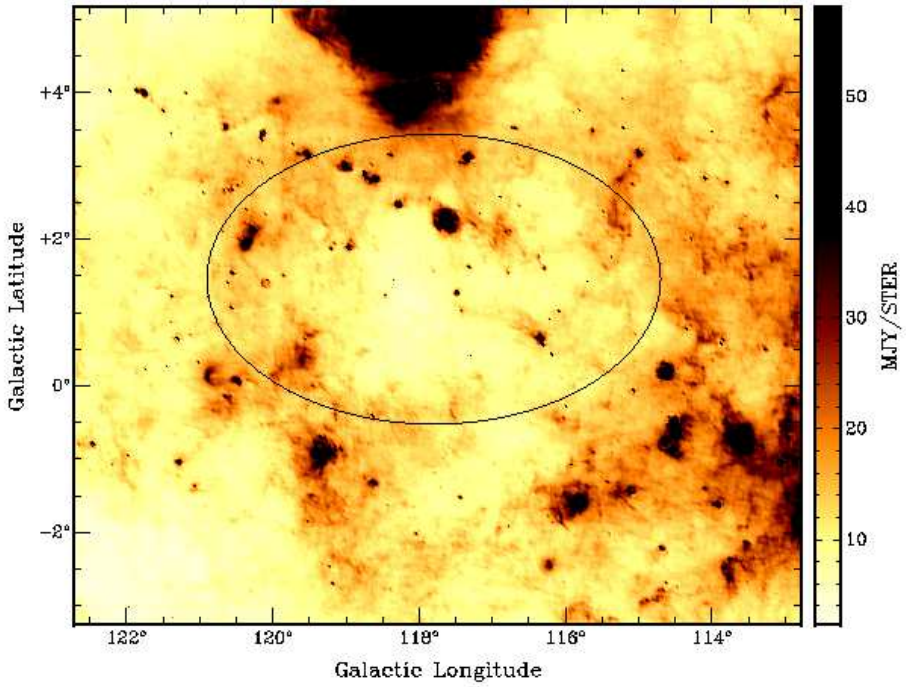


Figure 12. 60 μm HIRES IRAS data of the same area as Fig.11. The ellipse delineates the H I shell shown in Fig.10.

Cas OB5 (Garmany & Stencel 1992; Negueruela 2003). The total mechanical energy released by the stars during a time t is $E_w = (\Sigma 0.5\,\dot{M}\,v_\infty^2)\,t$, where $\dot{M}$ is the mass-loss rate and v_∞ the terminal velocity of the winds. The corresponding values were taken from Howarth & Prinja (1989) for the O-type stars (log $\dot{M}$ = –5.73, –6.76, –7.17, and –7.36; and v_∞ = 2800, 2200, 2100, and 2000 $\mathrm{km\,s^{-1}}$ for the O5, O8, O9, and O9.5 stars, respectively) and from van der Hucht, Cassinelli, & Williams (1986) and Prinja, Barlow, & Howarth (1990) for the WR star (log $\dot{M}$ = –4.5 and v_∞ = 1900 $\mathrm{km\,s^{-1}}$). We obtained that the total energy input due to the stellar winds is about $E_w = 1.3 \times 10^{45}\,t(\mathrm{yr})$ erg.

The total kinetic energy stored in the shell is $E_k = 0.5\,M_{\rm sh}\,V_{\rm exp}^2$, where $M_{\rm sh}$ is the total mass in the shell and $V_{\rm exp}$ the expansion velocity. We estimated the expansion velocity of the shell to be 16 ± 2 $\mathrm{km\,s^{-1}}$. Following the procedures described in Sections 3.3 and 3.4, we obtained the H I and molecular masses in the shell. Each mass was computed from the corresponding averaged image covering the velocity range from –20 to –50 $\mathrm{km\,s^{-1}}$. Adopting for GSH 117.8+1.5-35 a distance of 2 kpc, the total swept up mass is $M_{\rm sh} = (8 \pm 4) \times 10^5 M_\odot$, which is consistent with the value estimated by Moór & Kiss (2003) of 7.5 $\times 10^5 M_\odot$ (for their adopted distance of 2.5 kpc, which implies a mass of 4.8 $\times 10^5 M_\odot$ for a distance of 2 kpc). Thus, the kinetic energy of the shell is $E_k = (2 \pm 1) \times 10^{51}$ erg.

The theoretical model of Weaver et al. (1977) estimates that the efficiency of conversion of mechanical wind energy E_w into kinetic energy of the shell E_k is up to 20 % for the energy conserving model. This implies that the massive stars have to be acting during at least 8 Myr to create the shell. This value is larger than the lifetime of an O-type star and suggests that the five massive stars can not alone generate such a shell and other sources of energy should be considered. As suggested by Fich (1986), the supernova remnants located within the H I shell may be actively enlarging it. Out of the four SNRs located in the area, G114.3+0.3 is projected outside the H I shell and it is located at a distance of about 700 pc (Yar-Uyaniker, Uyaniker, & Kothes 2004). G114.3+0.3 and CTB1 have a distance estimate of about 1.6 kpc (Yar-Uyaniker et al. 2004), while Tycho is located at about 2.4 kpc (Lee, Koo, & Tatematsu 2004). Thus, assuming that there are three SNR possibly related to the shell and that each of them has injected 10^{51} erg, then the massive stars have to be acting during at least 5 Myr, which is consistent with the dynamical age estimated for the large shell. It is important to note that given the large errors involved in these estimations, the possibility that other sources of energy (stellar winds and/or supernova explosions) would have contributed in the formation of the shell can not be discarted. For instance, it is highly probable that the progenitors of the three SNR have contributed in the creation of the shell.

All the evidence shown above suggests that Sh2-173 is part of a hierarchical system of three generations. The members of Cas OB5 would have formed the large H I shell, whose expansion would have triggered the formation of the H II region Sh2-173, which in turn is triggering new stars in the surrounding molecular material. The fact that Sh2-173 is one of several young H II regions lying at the edge of the H I shell (see Fig.11) reinforces this conclusion. For example, Sh2-170 has been analyzed by Roger et al.

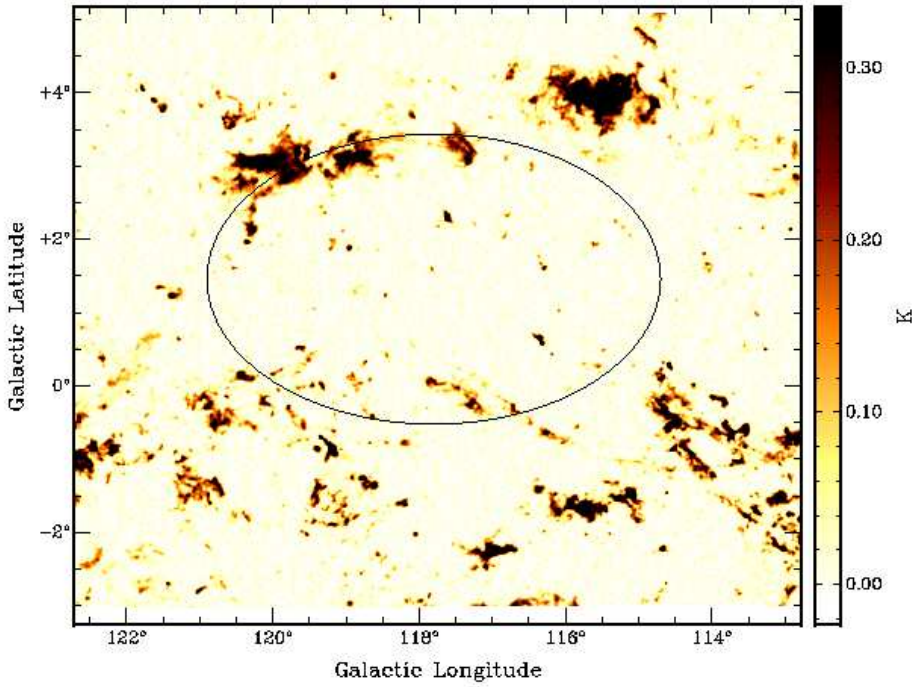


Figure 13. Averaged CO emission distribution in the velocity range from –50 to –20 $\mathrm{km\,s^{-1}}$. The ellipse delineates the H I shell shown in Fig.10.

(2004), who derived an age of $(2.5 - 5) \times 10^5$ yr, while Sh2-168 is considered as a compact H II region by Kothes & Kerton (2002). A detailed study of the H II regions shown in Fig. 11 would be useful to better understand the importance that the expansion of the large H I shell had in the process of triggering the formation of new generations of massive stars.

6 CONCLUSIONS

The H II region Sh2-173 has been analyzed in order to study the phenomena associated with the interaction of massive stars and the interstellar medium, and specifically, the process of triggering star formation. The analysis of the available radio continuum data have enabled us to estimate some parameters that characterize the H II region, like the ionized mass, the emission measure, and the electron density. From the radio flux densities estimated at different wavelengths, the thermal nature of the source was confirmed by the estimation of the spectral index $\alpha = 0.0 \pm 0.1$, $S_\nu \sim \nu^\alpha$. We noted that the massive stars present in the field can provide the necessary UV photon flux to keep the H II region ionized and heat the dust. As expected for H II regions, Sh2-173 displays a strong correlation between the 1420 MHz brightness temperature and infrared emission. An inspection of the H I images has shown the existence of an H I cavity which presents a good morphological agreement with the ionized gas. The H I feature is observed within the velocity range –24.6 and –31.6 $\mathrm{km\,s^{-1}}$ and has a systemic velocity of $-27.0 \pm 1.3\ \mathrm{km\,s^{-1}}$, compatible with the velocity of the ionized gas as obtained from Hα observations. The distribution of the MSX emission at 8.3 μm clearly shows the presence of a PDR bordering the brightest part of the H II region. Molecular gas probably related to Sh2-173 is observed in the velocity range –27.4 to –40.6 $\mathrm{km\,s^{-1}}$. Particularly, the CO feature named cloud A is clearly observed encircling both the H II region and the PDR. Applying different colour criteria, 46 YSO candidates have been identified in the vicinity of Sh2-173. Their positions in the CC and CM diagrams, as well as their correlation with molecular emission highly suggest the presence of an active star formation process in the molecular envelope of Sh2-173.

An analysis of the H I distribution in a larger area shows that Sh2-173 is located at the edge of a large shell, together with several other H II regions. This morphology suggests that Sh2-173 may be part of a hierarchical system of three generations. In this context, the age of the different structures were estimated. Based on evolutionary models of H II regions, we estimated for Sh2-173 a dynamical age of 0.6 - 1.0 Myr. As for the large H I shell, we have obtained a dynamical age $t_{\rm dyn} = 5 \pm 1$ Myr. Based on energetics considerations, we have concluded that the massive stars belonging to Cas OB5 could not alone create the shell, being highly probable that at least three supernova explosions have contributed in its formation. The obtained age difference between Sh2-173 and the H I shell, together with their relative location, lead us to the conclusion that Sh2-173 may have been created as a consequence of the action of a strong shock produced by the expansion of GSH 117.8+1.5-35 into the surrounding molecular gas. The analysis of the ages and

distribution of the other H II regions observed in the area would be useful to confirm this scenario.

ACKNOWLEDGMENTS

We would like to acknowledge Dr. E.M. Arnal for very useful comments and suggestions. This research has made use of the NASA/ IPAC Infrared Science Archive, which is operated by the Jet Propulsion Laboratory, California Institute of Technology, under contract with the National Aeronautics and Space Administration. The CGPS is a Canadian project with international partners and is supported by grants from NSERC. Data from the CGPS is publicly available through the facilities of the Canadian Astronomy Data Centre (http://cadc.hia.nrc.ca) operated by the Herzberg Institute of Astrophysics, NRC. The WENSS project is a collaboration between the Netherlands Foundation for Research in Astronomy (NFRA/ASTRON) and the Leiden Observatory WENSS team. This research has made use of the SIMBAD database, operated at CDS, Strasbourg, France. This project was partially financed by the Consejo Nacional de Investigaciones Científicas y Técnicas (CONICET) of Argentina under projects PIP 5886 and PIP 6433, Agencia PICT 00812, UBACyT X482, and UNLP 11/G072. We are grateful to the referee, whose suggestions led to the improvement of this paper.

REFERENCES

Arnal E. M., Corti M., 2007, A&A, 476, 255
Blitz L., Fich M., Stark A. A., 1982, ApJS, 49, 183
Bohlin R. C., Savage B. D., Drake J. F., 1978, ApJ, 224, 132
Brand J., Blitz L., 1993, A&A, 275, 67
Cappa C., Niemela V. S., Amorín R., Vasquez J., 2008, A&A, 477, 173
Cazzolato F., Pineault S., 2003, AJ, 125, 2050
Chan G., Fich M., 1995, AJ, 109, 2611
Condon J. J., Broderick J. J., Seielstad G. A., Douglas K., Gregory P. C., 1994, AJ, 107, 1829
Condon J. J., Cotton W. D., Greisen E. W., Yin Q. F., Perley R. A., Taylor G. B., Broderick J. J., 1998, AJ, 115, 1693
Cutri R. M., et., al,, 2003, 2MASS All Sky Catalog of point sources. The IRSA 2MASS All-Sky Point Source Catalog, NASA/IPAC Infrared Science Archive. http://irsa.ipac.caltech.edu/applications/Gator/
Dale J. E., Bonnell I. A., Whitworth A. P., 2007, MNRAS, 375, 1291
Deharveng L., Zavagno A., 2008, in Astronomical Society of the Pacific Conference Series, Vol. 387, Massive Star Formation: Observations Confront Theory, Beuther H., Linz H., Henning T., eds., pp. 338–+
Deharveng L., Zavagno A., Caplan J., 2005, A&A, 433, 565
Digel S. W., Hunter S. D., Mukherjee R., 1995, ApJ, 441, 270
Douglas J. N., Bash F. N., Bozyan F. A., Torrence G. W., Wolfe C., 1996, AJ, 111, 1945
Draine B. T., 1990, in Astrophysics and Space Science Library, Vol. 161, The Interstellar Medium in Galaxies, Thronson Jr. H. A., Shull J. M., eds., pp. 483–492
Drilling J. S., Landolt A. U., 2000, Normal Stars, Allen's Astrophysical Quantities, pp. 381–+
Dyson J. E., Williams D. A., 1980, Physics of the interstellar medium. New York, Halsted Press, p. 204
Egan M. P., et., al,, 2003, VizieR Online Data Catalog, 5114
Elmegreen B. G., 1998, in Astronomical Society of the Pacific Conference Series, Vol. 148, Origins, Woodward C. E., Shull J. M., Thronson Jr. H. A., eds., pp. 150–+
Elmegreen B. G., Lada C. J., 1977, ApJ, 214, 725
Fich M., 1986, ApJ, 303, 465
Fich M., Dahl G. P., Treffers R. R., 1990, AJ, 99, 622
Foster T., Routledge D., 2003, ApJ, 598, 1005
Fowler J. W., Aumann H. H., 1994, in Science with High Spatial Resolution Far-Infrared Data, Terebey S., Mazzarella J. M., eds., p. 1
Fürst E., Reich W., Reich P., Reif K., 1990, A&AS, 85, 691
Garmany C. D., Stencel R. E., 1992, A&AS, 94, 211
Georgelin Y. M., 1975, PhD thesis, , Univ. Provence, Obs. de Marseille, (1975)
Grenier I. A., Lebrun F., 1990, ApJ, 360, 129
Heyer M. H., Brunt C., Snell R. L., Howe J. E., Schloerb F. P., Carpenter J. M., 1998, ApJS, 115, 241
Hosokawa T., Inutsuka S.-i., 2006, ApJ, 646, 240
Howarth I. D., Prinja R. K., 1989, ApJS, 69, 527
Humphreys R. M., 1976, ApJ, 206, 114
Junkes N., Fürst E., Reich W., 1992, A&A, 261, 289
Kenyon S. J., Hartmann L., 1995, ApJS, 101, 117
Kerber F., Mignani R. P., Guglielmetti F., Wicenec A., 2003, VizieR Online Data Catalog, 340, 81029
Kerton C. R., Arvidsson K., Knee L. B. G., Brunt C., 2008, MNRAS, 385, 995
Kirsanova M. S., Sobolev A. M., Thomasson M., Wiebe D. S., Johansson L. E. B., Seleznev A. F., 2008, MNRAS, 388, 729
Kiss C., Moór A., Tóth L. V., 2004, A&A, 418, 131
Klein R. I., Sandford II M. T., Whitaker R. W., 1980, Space Science Reviews, 27, 275
Kothes R., Kerton C. R., 2002, A&A, 390, 337
Lee J.-J., Koo B.-C., Tatematsu K., 2004, ApJ, 605, L113
Lefloch B., Lazareff B., 1994, A&A, 289, 559
—, 1995, A&A, 301, 522
Lumsden S. L., Hoare M. G., Oudmaijer R. D., Richards D., 2002, MNRAS, 336, 621
Martins F., Plez B., 2006, A&A, 457, 637
Martins F., Schaerer D., Hillier D. J., 2005, A&A, 436, 1049
McCray R., Kafatos M., 1987, ApJ, 317, 190
Mezger P. G., Henderson A. P., 1967, ApJ, 147, 471
Moór A., Kiss C., 2003, Communications of the Konkoly Observatory Hungary, 103, 149
Negueruela I., 2003, A&A, 408, 689
Oey M. S., Watson A. M., Kern K., Walth G. L., 2005, AJ, 129, 393
Patel N. A., Goldsmith P. F., Heyer M. H., Snell R. L., Pratap P., 1998, ApJ, 507, 241
Pineault S., 1998, AJ, 115, 2483
Price S. D., Egan M. P., Carey S. J., Mizuno D. R., Kuchar T. A., 2001, AJ, 121, 2819
Prinja R. K., Barlow M. J., Howarth I. D., 1990, ApJ, 361, 607
Quireza C., Rood R. T., Bania T. M., Balser D. S., Maciel W. J., 2006, ApJ, 653, 1226
Rengelink R. B., Tang Y., de Bruyn A. G., Miley G. K., Bremer M. N., Roettgering H. J. A., Bremer M. A. R., 1997, A&AS, 124, 259
Rieke G. H., Lebofsky M. J., 1985, ApJ, 288, 618
Robitaille T. P., Whitney B. A., Indebetouw R., Wood K., Denzmore P., 2006, ApJS, 167, 256

Roger R. S., McCutcheon W. H., Purton C. R., Dewdney P. E., 2004, A&A, 425, 553
Russeil D., Adami C., Georgelin Y. M., 2007, A&A, 470, 161
Sandford II M. T., Whitaker R. W., Klein R. I., 1982, ApJ, 260, 183
Schaerer D., de Koter A., 1997, A&A, 322, 598
Sharpless S., 1959, ApJS, 4, 257
Skrutskie M. F., et., al,, 2006, AJ, 131, 1163
Taylor A. R., et., al,, 2003, AJ, 125, 3145
Thé P. S., de Winter D., Perez M. R., 1994, A&AS, 104, 315
Thompson M. A., White G. J., Morgan L. K., Miao J., Fridlund C. V. M., Huldtgren-White M., 2004, A&A, 414, 1017
Tokunaga A. T., 2000, Infrared Astronomy, Allen's Astrophysical Quantities, pp. 143–+
Vacca W. D., Garmany C. D., Shull J. M., 1996, ApJ, 460, 914
van der Hucht K. A., Cassinelli J. P., Williams P. M., 1986, A&A, 168, 111
Weaver H., Williams D. R. W., 1973, A&AS, 8, 1
Weaver R., McCray R., Castor J., Shapiro P., Moore R., 1977, ApJ, 218, 377
Whitworth A. P., Bhattal A. S., Chapman S. J., Disney M. J., Turner J. A., 1994, MNRAS, 268, 291
Yar-Uyaniker A., Uyaniker B., Kothes R., 2004, ApJ, 616, 247